

A LABOCA survey of the Extended Chandra Deep Field South – submillimeter properties of near-infrared selected galaxies

T.R. Greve¹, A. Weiß², F. Walter¹, I. Smail³, X.Z. Zheng⁴, K.K. Knudsen⁵, K.E.K. Coppin³, A. Kovács², E.F. Bell¹, C. de Breuck⁶, H. Dannerbauer¹, M. Dickinson⁷, E. Gawiser⁸, D. Lutz⁹, H.-W. Rix¹, E. Schinnerer¹, D. Alexander³, F. Bertoldi⁵, W.N. Brandt¹⁰, S.C. Chapman¹¹, R.J. Ivison¹², A.M. Koekemoer¹³, E. Kreysa², P. Kurczynski⁸, K. Menten², G. Siringo², M. Swinbank³, P. van der Werf¹⁴

tgreve@mpia-hd.mpg.de

ABSTRACT

Using the 330 hr ESO-MPG 870- μm survey of the Extended Chandra Deep Field South (ECDF-S) obtained with the Large Apex BOlometer CAmera (LABOCA) on the Atacama Pathfinder EXperiment (APEX), we have carried out a stacking analysis at submillimeter (submm) wavelengths of a sample of 8266 near-infra-red (near-IR) selected ($K_{\text{vega}} \leq 20$) galaxies, including 893 BzK galaxies, 1253 extremely red objects (EROs) and 737 distant red galaxies (DRGs), selected from the Multi-wavelength Survey by Yale-Chile (MUSYC). We measure average 870- μm fluxes of 0.20 ± 0.01 mJy (20.0σ), 0.45 ± 0.04 mJy (11.3σ), 0.42 ± 0.03 mJy (14.0σ), and 0.41 ± 0.04 mJy (10.3σ) for the $K_{\text{vega}} \leq 20$, BzK, ERO and DRG samples, respectively. For the BzK, ERO and DRG subsamples, which overlap to some degree and are like to be at $z \simeq 1 - 2$, this implies an average far-IR luminosity of $\sim 2 - 6 \times 10^{11} L_{\odot}$ and star formation rate of $\sim 40 - 100 M_{\odot}$. Splitting the BzK galaxies up into star-forming (sBzK) and passive (pBzK) galaxies, the former is significantly detected (0.48 ± 0.04 mJy, 12.0σ) while the latter is only marginally detected (0.27 ± 0.10 mJy, 2.7σ), thus confirming that the sBzK/pBzK criteria do isolate obscured, star forming and truly passive galaxies. The $K_{\text{vega}} \leq 20$ galaxies are found to contribute with 6.6 ± 0.3 Jy deg^{-2} ($\sim 15\%$) to the 870- μm extragalactic background light (EBL). sBzK and pBzK galaxies contribute 1.7 ± 0.2 Jy deg^{-2} ($\sim 4\%$) and 0.2 ± 0.1 Jy deg^{-2} ($< 0.5\%$) to the EBL. We present the first delineation of the average submm signal from $K_{\text{vega}} \leq 20$ selected galaxies and their contribution to the submm EBL as a function of (photometric) redshift, and find a decline in the average submm signal (and therefore IR luminosity and star formation rate) by a factor $\sim 2 - 3$ from $z \sim 2$ to $z \sim 0$. This is in line with a cosmic star formation history in which the star formation activity in galaxies increases significantly at $z \gtrsim 1$. A linear correlation between the average 24- μm and 870- μm flux densities is found for $K_{\text{vega}} \leq 20$ galaxies with 24- μm fluxes $\lesssim 350 \mu\text{Jy}$ (corresponding to $L_{\text{IR}} \simeq 1.5 \times 10^{12} L_{\odot}$ at $z \simeq 2$), while at higher 24- μm fluxes there is no correlation. This behaviour suggests that star formation, and not Active Galactic Nuclei (AGN), is in general responsible for the bulk of the mid-IR emission of $L_{\text{IR}} \lesssim 1.5 \times 10^{12} L_{\odot}$ systems, while in more luminous systems the AGN makes a significant contribution to the 24- μm emission. By mapping the stacked 870- μm signal across the $B - z$ vs. $z - K$ diagram we have confirmed the ability of the sBzK-selection criterion to select starforming galaxies at $z > 1$, although our analysis suggest that the subset of sBzK galaxies which are also EROs are responsible for $> 80\%$ of the submm emission from the entire sBzK population.

Subject headings: cosmology: observations — galaxies: evolution — galaxies: formation — galaxies: high-redshift

1. Introduction

Extragalactic blank-field submm surveys have been carried out since the advent of SCUBA (Holland 1999) more than a decade ago, and have provided us with a unique view of intense, dust-cloaked star formation events at high redshifts (e.g. Blain et al. 2002). Yet such observations have so far only pin-pointed the most luminous high- z galaxies, due to the limitations in sensitivity and resolution imposed by preset-day (sub)mm facilities. It is now well-established that the bright ($\gtrsim 5$ mJy at $850\text{-}\mu\text{m}$) submm sources uncovered by these surveys primarily reside in the redshift range $z \simeq 1.5 - 3.5$ (Chapman et al. 2003, 2005), and account for $\sim 20 - 30$ percent of the extragalactic background light (EBL) at $850\text{-}\mu\text{m}$ (Barger et al. 1998, 1999; Hughes et al. 1998; Coppin et al. 2006). Surveys that make use of galaxy clusters' gravitational amplification of the background source plane have uncovered a number of faint ($S_{850\mu\text{m}} \gtrsim 2$ mJy) sources and resolved up to 80 per-cent of the background (Smail et al. 1997, 2002a; Blain et al. 1999; Cowie et al. 2002; Chapman et al. 2002; Knudsen et al. 2008). However, we know little about the nature and redshift dis-

tribution (Smail et al. 1997, 2002a) of the population below ~ 5 mJy due in part to the difficulty of identifying counterparts in the radio.

The recent advent of large format near-IR cameras have revealed populations of moderately star forming galaxies at $z \simeq 1 - 3$ that are more numerous than the (sub)mm selected systems, and more representative of the bulk population at these epochs (e.g. Cimatti et al. 2002; Lawrence et al. 2007). The rest-frame near-IR is arguably the best wavelength range to undertake such surveys at – as, in comparison with UV and optical surveys, it is less sensitive to the effects of age and dust on the stellar population, and thus more closely provides a selection based on stellar mass.

Well known examples of near-IR colour-selected galaxies are the populations of extremely red objects (EROs – Elston, Rieke & Rieke 1988, McCarthy, Persson & West 1992; Hu & Ridgway 1994), distant red galaxies (DRGs – Franx et al. 2003; van Dokkum et al. 2003), and the so-called BzK galaxies (Daddi et al. 2004). While these populations are selected according to different optical/near-IR colour criteria applied, which pick out systems at different, but overlapping, redshift ranges. These colour criteria are often designed to straddle the 4000\AA break (including the Balmer break at 3646\AA), characteristic of evolved, metal-enriched galaxies that are old enough that OB-stars do not dominate the light. The same colour criteria, however, will also select dusty, starforming galaxies at virtually any redshift. Thus, near-IR colour-selected galaxy populations are typically a mix of actively star forming galaxies and old, evolved systems, which means additional colour criteria and/or spectral analysis has to be applied in order to separate the two. Clearly, submm observations offer a unique way of distinguishing between starforming and passive near-IR galaxies.

At present, however, the bulk of near-IR colour-selected galaxies are too faint for individual detection by large format (sub)mm surveys, and for the moment, therefore, the only way forward is to study their average (sub)mm/far-IR properties by means of stacking techniques. A handful of such studies have been carried out to date, characterizing the average submm signal of near-IR selected galaxies and their contribution to the extragalactic background light (EBL) at submm

¹Max-Planck-Institut für Astronomie, 69117 Heidelberg, Germany

²Max-Planck-Institut für Radioastronomie, D-53121 Bonn, Germany

³Institute for Computational Cosmology, Durham University, Durham DH1 6BH, UK

⁴Purple Mountain Observatory, Chinese Academy of Sciences, Nanjing 210008, China

⁵Argelander Institute for Astronomy, University of Bonn, 53121 Bonn, Germany

⁶European Southern Observatory, Garching bei München, Germany

⁷National Optical Astronomical Observatory, Tucson, Arizona 85719, USA

⁸Physics & Astronomy Department, Rutgers University, Piscataway, NJ 08854, USA

⁹Max-Planck-Institut für extraterrestrische Physik, 85741 Garching bei München, Germany

¹⁰Pennsylvania State University, Astronomy and Astrophysics 525 Davey Lab, University Park, PA 16802, USA

¹¹Institute for Astronomy, Cambridge CB3 0HA, UK

¹²UK Astronomy Technology Centre, Royal Observatory, Edinburgh EH9 3HJ, UK

¹³Space Telescope Science Institute, Baltimore, Maryland 21218, USA

¹⁴Leiden Observatory, PO Box 9513, 2300 RA Leiden, The Netherlands

wavelengths (Webb et al. 2004; Daddi et al. 2005; Knudsen et al. 2005; Takagi et al. 2007). Yet most of these stacking analyses have been of relatively small samples of galaxies, and as a consequence have had to averaging their submm properties over the entire redshift range from which they are selected (which is often substantial, $z \sim 1 - 3$). A robust delineation of the submm signal of near-IR selected galaxies as a function of redshifts has therefore been lacking, and as a consequence we do not know how the dust-enshrouded starformation in these galaxies evolve with cosmic epoch.

The Extended Chandra Deep Field South (ECDF-S), a $30' \times 30'$ region centered on the smaller GOODS-S/CDF-S field (Giavalisco et al. 2004), is one of the most intensively studied extragalactic fields in the southern sky. In addition to X-ray observations with Chandra (Alexander et al. 2003; Lehmer et al. 2005; Luo et al. 2008), the EDCF-S has been targeted in a large number of optical and near-IR filter passbands from the ground as part of COMBO-17 (Wolf et al. 2001) and MUSYC (Gawiser et al. 2003), and with HST/ACS as part of GEMS (Rix et al. 2004). Furthermore, deep mid-IR imaging has been provided by the *Spitzer* IRAC/MUSYC Public Legacy in ECDF-S (SIMPLE, Damen et al. 2009), and the *Spitzer*/MIPS Far-Infrared Deep Extragalactic Legacy Survey (FIDEL – Dickinson et al. in prep. See also <http://ssc.spitzer.caltech.edu/legacy/abs/dickinson2.html>).

To study the submm properties of the sources in the ECDF-S, we have undertaken a large ESO-MPG survey (Coppin et al. 2009; Weiß et al. 2009) using the LABOCA 870- μ m camera (Siringo et al. 2009) mounted on the Atacama Pathfinder Experiment (APEX) and combined the data with the already existing multi-wavelength data available for this field.

Throughout this paper we adopt a flat cosmology with $\Omega_M = 0.27$, $\Omega_\Lambda = 0.73$, and $h = 0.71$ (Spergel et al. 2003).

2. The submm data

Observations were carried out using the 295 horn-bolometer array LABOCA on APEX (Siringo et al. (2009), and are discussed in detail in Weiß et al. (2009)). The bolometers are AC-biased, op-

erated in total power mode, and distributed in a hexagonal configuration over the $11.4'$ field of view. The center frequency of LABOCA is 345 GHz and its passband has a FWHM of ~ 60 GHz. The measured angular resolution is $19.2''$ (FWHM). The observations were carried out between May 2007 and November 2008 in mostly excellent weather conditions (PWV typically 0.5 mm corresponding to a zenith opacity of 0.2 at the observing wavelength). The mapping pattern was chosen to give a uniform coverage across a $30' \times 30'$ area centered at Ra: $03^h32^m29^s$ Dec $-27^\circ48'47''$ (J2000).

Mapping was performed alternating rectangular on-the-fly scans with raster of spiral patterns. For the latter mode the telescope traces in two scans spirals with radii between $2'$ and $4'$ at 16 and 9 positions (the raster) spaced by $600''$ in azimuth and elevation. The scanning speed was typically between 2-3 arcmin per second.

Calibration was achieved through observations of Mars, Uranus and Neptune as well as secondary calibrators and was found to be accurate within 8.5%. The atmospheric attenuation was determined via skydips every ~ 2 hours as well as from independent data from the APEX radiometer which measures the line of sight water vapor column every minute. Focus settings were typically determined once per night and checked during sunrise. Pointing was checked on nearby quasars PMNJ0457-2324, PMNJ0106-4034 and PMNJ0403-3605 and found to be stable within $3''$.

The data was reduced using the BoA reduction package (Schuller et al. in prep.). Individual maps were co-added (noise-weighted) and the final map was beam-smoothed, resulting in a spatial resolution of $27''$ (FWHM). The total on-source observing time in the data used for this analysis is 200 hours (330 hr including overheads) and the average rms across the entire $30' \times 30'$ field is $1.2 \text{ mJy beam}^{-1}$, making it the largest contiguous (sub)mm survey ever undertaken to this depth (c.f. Coppin et al. 2006; Bertoldi et al. 2007).

3. Near-IR selected galaxies

We use the Wide MUSYC public data release of *UBVRIzJHK* catalogues in the ECDF-S to construct samples of near-IR selected galaxies (Taylor

et al. 2008)¹. The MUSYC survey covers the central $30' \times 30'$ of the ECDF-S and reaches $5\text{-}\sigma$ point source sensitivities in the near-IR of $J_{\text{AB}} = 22.7$ and

4. Near-IR selected galaxies

We use the Wide MUSYC public data release of *UBVRIZJHK* catalogues in the ECDF-S to construct samples of near-IR selected galaxies (Taylor et al. 2008)². The MUSYC survey covers the central $30' \times 30'$ of the ECDF-S and reaches $5\text{-}\sigma$ point source sensitivities in the near-IR of $J_{\text{AB}} = 22.7$ and $K_{\text{AB}} = 22.0$, respectively (see Gawiser et al. (2006) for a detailed description of the MUSYC survey).

We defined our sample as sources with $K_{\text{vega}} \leq 20$ (corresponding to $K_{\text{AB}} \leq 21.9$, i.e. we have assumed a VEGA-AB offset of 1.9 in the K -band). This magnitude cut-off was chosen since the MUSYC survey is close to 100% complete at this depth, and since other studies have adopted the same magnitude limit, thus facilitating a direct comparison. Contamination by stars was accounted for by removing objects lying on the stellar loci in the $(z - K)_{\text{AB}}$ vs. $(B - z)_{\text{AB}}$ or $(J - K)_{\text{AB}}$ vs. $(R - K)_{\text{AB}}$ diagrams (hereafter referred to as BzK and RJK diagrams – Fig. 1). As shown in Fig. 1a and b, a non-negligible fraction of sources that appear as normal galaxies in the BzK diagram end up in the stellar region in the RJK diagram and vice versa. These sources were all poorly fit ($\chi^2/\nu_{\text{dof}} > 100$) by galaxy SED templates, thus strongly suggesting that they are in fact stars and illustrating the need of removing both stellar loci from the sample. This left us with a total sample of 8266 $K_{\text{vega}} \leq 20$ selected galaxies. From this sample, subsets of BzK galaxies, extremely red objects (EROs) and distant red galaxies (DRGs) were extracted as described below.

Applying the star-forming and passive BzK criteria, namely $BzK = (z - K)_{\text{AB}} - (B - z)_{\text{AB}} \geq -0.2$ for sBzK galaxies, and $BzK < -0.2$ and $(z - K)_{\text{AB}} > 2.5$ for pBzK galaxies (Daddi et al. 2004), to our $K_{\text{vega}} \leq 20$ catalogue defined above,

we obtained samples of 744 sBzK and 149 pBzK galaxies³. Sources which were undetected at the 1σ level in both B and z were not included. Furthermore, sources formally belonging to the sBzK-region but which were undetected in B , thus having $B - z$ lower limits only, were discarded, as were sources in the pBzK region with lower limits in $z - K$. A total of 1253 EROs were selected from our $K_{\text{vega}} \leq 20$ sample using the standard criterion, i.e. $(R - K)_{\text{AB}} \geq 3.35$ (equivalent to $(R - K)_{\text{vega}} \gtrsim 5$ – Elston, Rieke & Rieke 1988; McCarthy, Persson & West 1992; Hu & Ridgeway 1994). Finally, the selection of DRGs was done by applying the colour cut $(J - K)_{\text{AB}} > 1.32$ (Franz et al. 2003). In total 737 DRGs with $K_{\text{vega}} \leq 20$ were selected in this way.

4.1. Overlap between BzK, ERO, and DRG samples

In this paper we aim to determine the contribution to the submm background from $K_{\text{vega}} \leq 20$ galaxies, as well as the sub-samples of BzKs, EROs and DRGs and their joint contributions, and it is therefore important to determine the degree of overlap between these populations. The overlaps in terms of percentages are given in Table 1.

From Fig. 2 it is seen that BzK, ERO and DRG galaxies only start to contribute significantly ($> 1\%$) to the full sample for $K_{\text{AB}} \gtrsim 20$. Even so, more than half of the full sample does not fall within the BzK/ERO/DRG classifications at these faint flux levels. Of the full $K_{\text{vega}} \leq 20$ sample, 6269 sources (corresponding to $\sim 76\%$) do not classify as BzKs, EROs or DRGs.

The locations of the various samples in the BzK and RJK diagrams are shown in Fig. 1. The DRGs are seen to be spread out across the BzK diagram, while the EROs lie in a much more well defined region of the BzK diagram. EROs and DRGs make up about 30% and 36% of the sBzKs, respectively. Similarly, we find that EROs and DRGs constitute 98% and 44% of the pBzK sample, respectively. Clearly, pBzK galaxies are much more often selected as EROs than is the case for sBzKs, while the occurrence of a pBzK or sBzK galaxy being classified as a DRG is about the same. Turning to the RJK-diagram we see that the sBzK galax-

¹The catalogue is available at <http://www.astro.yale.edu/MUSYC/>

²The catalogue is available at <http://www.astro.yale.edu/MUSYC/>

³We matched the stellar sequence in the BzK-diagram with that of Daddi et al. (2004) using $(z - K)_{D04} = (z' - K) - 0.2$.

TABLE 1

THE TOTAL NUMBER OF SOURCES IN EACH SAMPLE (GIVEN IN PARENTHESES IN THE FIRST COLUMN OF EACH LINE), FOLLOWED BY THE PERCENTAGES CONTRIBUTED BY THE OTHER SAMPLES. THE LATTER ARE ALSO GIVEN AS ABSOLUTE NUMBERS IN PARENTHESES.

	sBzK	pBzK	ERO	DRG	sBzK+pBzK	ERO+DRG
$K_{\text{vega}} \leq 20$ (8266)	9%(744)	1.8%(149)	15.2%(1253)	8.9%(737)	10.8%(893)	19.6%(1620)
sBzK (744)	100%(744)	0%(0)	30.4%(226)	36.2%(269)	83.3%(744)	49.7%(370)
pBzK (149)	0%(0)	100%(149)	98.0%(146)	43.6%(65)	16.7%(149)	98%(146)
ERO (1253)	18.0%(226)	11.7%(146)	100%(1253)	29.5%(370)	29.7%(372)	100%(1253)
DRG (737)	36.5%(269)	8.8%(65)	50.2%(370)	100%(737)	45.3%(334)	100%(737)
sBzK+pBzK (893)	83.3%(744)	16.7%(149)	41.7%(372)	37.4%(334)	100%(893)	57.8%(516)
ERO+DRG (1620)	22.8%(370)	9.0%(146)	63.0%(1253)	37.0%(737)	31.9%(516)	100%(1620)

ies are much more spread out than the pBzKs. About 18% and 37% of EROs and DRGs, respectively, are made up of sBzK, while pBzKs make up about 12% and 9% of the two populations.

The overlaps between BzK, ERO and DRG galaxies have been discussed in detail in other studies (e.g. Reddy et al. 2005; Grazian et al. 2007; Takagi et al. 2007; Lane et al. 2008). The most statistically significant study was carried out by Lane et al. (2009) who used the UKIRT Infrared Deep Sky Survey (UKIDSS) Ultra Deep Survey Early Data Release (UDS EDR) to study large samples of BzK, ERO and DRG galaxies. For samples selected down to $K_{\text{AB}} = 21.2$, which is close to our magnitude cut-off, they found sBzK:ERO and pBzK:ERO ratios of 32% and 95%, respectively, i.e. in excellent agreement with our values. They also find that about 30% of DRGs are sBzK, again in good agreement with our findings (see also Reddy et al. 2005).

4.2. Redshift distributions

The sample was correlated against publically available spectroscopic redshift surveys (Szokoly et al. 2004; Vanzella et al. 2005, 2006, 2008; Popesso et al. 2008; Kriek et al. 2008). Using only the most reliable spectroscopic redshifts from these surveys we extracted 2341 redshifts, of which the majority lie within the CDF-S region. A total of 546 galaxies from our sample were matched to a spectroscopic redshift. Of these 28 were sBzK, 21 were ERO, and 10 were DRG galaxies. The fact that no pBzK galaxies were identified with a spectroscopic redshift is not too surprising since these are in all likelihood old, evolved galaxies with optical spectra devoid of emission features, thus mak-

ing it difficult to obtain robust spectroscopic redshifts (cf. Kriek et al. 2006; Cimatti et al. 2008). Sources with spectroscopic redshifts were used as a test sample to optimize input parameters for the photometric redshift code EAZY (Brammer, van Dokkum & Coppi 2008). The code works by fitting non-negative linear combinations of galaxy spectra to the observed spectral energy distributions (SEDs), which in our case consisted of the nine MUSYC filter bands.

The resulting photometric redshifts are compared against their spectroscopic counterparts in Fig. 3. The normalized median absolute deviation of $\Delta z = z_{\text{phot}} - z_{\text{spec}}$ (see Brammer, van Dokkum & Coppi 2008) is $\simeq 0.037$ for $z \leq 1.5$ and $\simeq 0.079$ for $z > 1.5$. Significant outliers, which we define to be sources with $|\Delta z|/(1 + z_{\text{spec}})$ 5 times greater than the median, make up $\sim 9\%$ of the total sample. These numbers are consistent with the typical performances of photometric redshift codes (e.g. Bolzonella, Miralles & Pelló 2000; Quadri et al. 2007; Brammer van Dokkum & Coppi 2008).

Adopting the parameters for the test sample, photometric redshifts were derived for the remainder of the sample without spectroscopic redshifts. The redshift distributions of the full $K_{\text{vega}} \leq 20$ sample as well as the BzK, ERO, and DRG samples are shown in Fig. 4, where we also compare with two other photometric redshift distributions obtained from: 1) the MUSYC UBVRi and deep JHK imaging of the three $10' \times 10'$ fields HDFS1/S2, MUSYC 1030 and 1255 (Quadri et al. 2007 - hereafter Q07), and 2) deep BVRi'z'JK imaging of 1113 arcmin^2 in the Ultra-Deep Survey (UDS) portion of the United Kingdom Infrared Telescope Deep Sky Survey (UKIDSS) (Dunne et

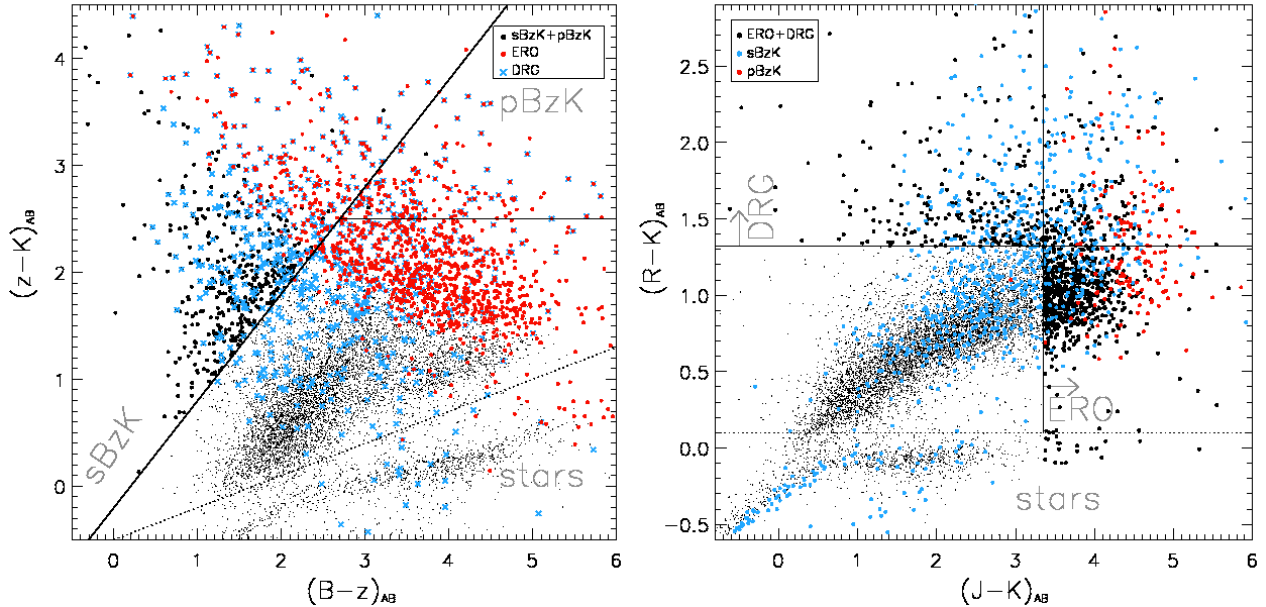


Fig. 1.— Colour-magnitude diagrams illustrating the selection criteria for the BzK, ERO and DRG samples. **Left:** The BzK-diagram (D04) showing the sBzK and pBzK regions and the location of sources selected according to the ERO- and DRG-criteria. **Right:** RJK diagram showing the ERO and DRG regions and the location of the sources fulfilling the sBzK and pBzK colour criteria. Sources below the dotted lines in either diagram were deemed to be stars and therefore discarded from the analysis. Note this includes a number of sources formally selected as either BzK, ERO or DRG galaxies (see § 4). The diagrams show the significant overlap between the different near-IR selected populations.

al. 2008 - hereafter D08).

The BzK selection criteria are defined to select galaxies in the redshifts range $1.4 < z < 2.5$ (Daddi et al. 2004), yet both the sBzK and pBzK redshift distributions extend below and above this range. Of the sBzK galaxies, 66 % lie in the range $1.4 < z < 2.5$, while 22 % are at $z < 1.4$ and 12 % at $z > 2.5$. For the pBzK galaxies, the corresponding percentages are 60 %, 31 %, and 9 %, respectively. Both Q07 and D08 find similar fractions for their samples of $K_{\text{vega}} \leq 20$ galaxies, suggesting that the BzK criteria select galaxies across a somewhat broader redshift range ($1 \lesssim z \lesssim 3.5$). The redshift distribution of EROs is seen to peak strongly at $z \simeq 1.1$ with a tail extending to $z \sim 3.5$. This is in line with photometric and spectroscopic surveys which have shown that the redshift distribution of EROs peaks around $z \simeq 1.2$ (Cimatti et al. 2003; Yan et al. 2004). The redshift distribution of $K_{\text{vega}} \leq 20$ EROs derived by D08 peaks at slightly higher redshifts ($z \sim 1.4$),

but overall appears similar to ours. The DRG distribution shows prominent peaks at $z \simeq 1.2$ and $z \simeq 2$, with the former being the most dominant. A similar bimodality is also apparent in the $K_{\text{vega}} \leq 20$ DRG sample by Q07, although the dominant peak in their distribution lies at $z \simeq 2$. The distribution by D08 broadly resembles ours, with a prominent peak at $z \simeq 1.2$ followed by a significant high- z tail. Overall, therefore, our redshift distributions are consistent with those of Q07 and D08, given the uncertainties associated with photometric redshift derivation, and the effects of field-to-field variations.

5. 870- μm Stacking

In order to estimate the average 870- μm fluxes for the above excised catalogues of near-IR galaxies we stack the 870- μm flux values at their near-IR positions in the LABOCA map.

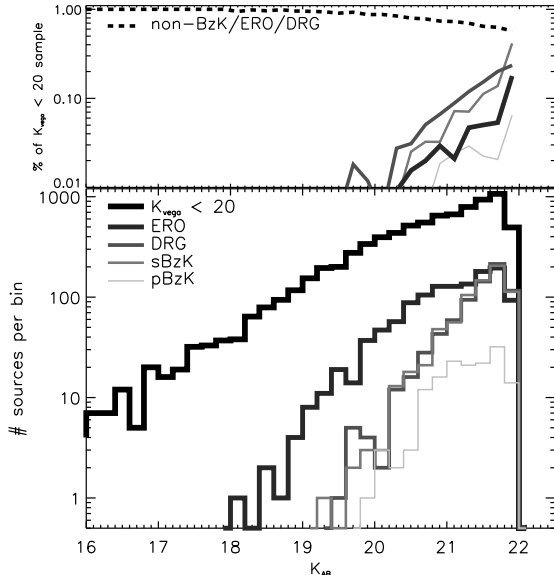


Fig. 2.— **Top:** Percentages, i.e. fraction of the full $K_{\text{vega}} \leq 20$ sample, of the BzK, ERO and DRG samples, as well as the non-BzK/ERO/DRG sample (dashed line) as a function of their K_{AB} magnitude. **Bottom:** The number distribution of sources as a function of their K_{AB} magnitude. The distributions for the full sample as well as the BzK, ERO and DRG samples are shown in order to illustrate the overlap between the different populations. While the BzK, ERO and DRG samples start making up a non-negligible fraction of the parent sample for $K_{\text{AB}} \gtrsim 20$, even at the faintest magnitudes more than half of the sources from the parent sample do not fall within any of these three classifications.

5.1. Submm-bright near-IR selected galaxies

First, however, we need to identify any galaxies which are associated with robust LABOCA sources, which we take to mean sources detected at $\geq 3.7\text{-}\sigma$ significance (see Weiß et al. 2009 for details). To this end we adopt a search radius of $12.8''$ around each LABOCA source, which corresponds to the 95 per-cent confidence search radius given the $\text{FWHM}=19''$ beam. For a galaxy to qualify as a near-IR counterpart to a LABOCA source, we furthermore require that $z > 0.8$. If more than one galaxy meets these criteria for a given LABOCA source, we adopt the one closest

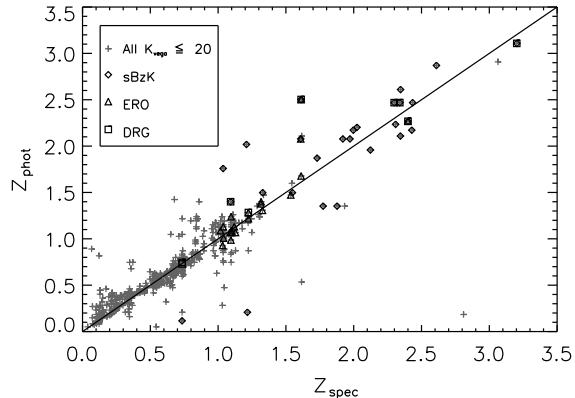


Fig. 3.— Photometric versus spectroscopic redshifts for the sources in the full $K_{\text{vega}} \leq 20$ sample, and the sBzK/pBzK, ERO and DRG sub-samples which have spectroscopic redshifts (see § 4.2). The normalized median absolute deviation of $\Delta z = z_{\text{phot}} - z_{\text{spec}}$ (see Brammer, van Dokkum & Coppi 2008) is $\simeq 0.037$ for $z \leq 1.5$ and $\simeq 0.079$ for $z > 1.5$.

to the submm source. In this manner we find 54 submm-near-IR associations from the $K_{\text{vega}} \leq 20$ sample. Of these, 17/2 sources are classified as sBzK/pBzK galaxies and 28 as EROs (of which 16 are also DRGs). 11 of the 17 sBzK galaxies are also EROs and of those, 9 are DRGs. Both of pBzK galaxies are EROs, and also DRGs. As a safeguard against contamination, these submm-bright near-IR sources were removed from the stacking analysis, although their contribution was included (in a variance-weighted fashion) in the final tally of average submm flux (Table 2).

5.2. Stacking and deblending technique

Next, we proceeded to perform a stacking analysis of the remaining submm-undetected near-IR selected galaxies. Due to the slightly varying noise across the map, the average $870\text{-}\mu\text{m}$ flux ($\langle S_{870\mu\text{m}} \rangle$) and noise ($\langle \sigma_{870\mu\text{m}} \rangle$) values were calculated as the variance-weighted mean, i.e.

$$\langle S_{870\mu\text{m}} \rangle = \frac{\sum_i S_i / \sigma_i^2}{\sum_i 1 / \sigma_i^2}, \quad (1)$$

and

$$\langle \sigma_{870\mu\text{m}} \rangle = \frac{1}{\sqrt{\sum_i 1 / \sigma_i^2}}, \quad (2)$$

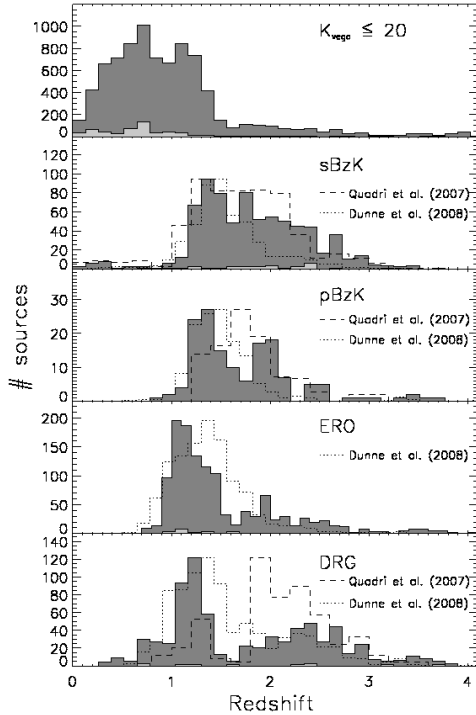


Fig. 4.— Top to bottom: redshift distributions of the $K_{\text{vega}} \leq 20$, sBzK, pBzK, ERO and DRG samples, respectively (dark grey histograms). Spectroscopic redshifts are shown as light grey histograms. Also shown are the photometric redshift distributions of the $K_{\text{vega}} \leq 20$ sBzK, pBzK and DRG samples by Q07, as well as of the $K_{\text{vega}} \leq 20$ selected samples by D08. The Q07 and D08 distributions have been scaled to match the peaks of our distributions. Given the uncertainties, our $K_{\text{vega}} \leq 20$ BzK, ERO and DRG redshift distributions are in good agreement with those of Q07 and D08.

where S_i and σ_i are the $870\text{-}\mu\text{m}$ flux and r.m.s. noise pixel values at the near-IR position of the i^{th} source in the stack, respectively. To avoid the stack being contaminated by robust $870\text{-}\mu\text{m}$ sources, the stacking was performed on a ‘residual’ version of the LABOCA map in which all of the 55 $870\text{-}\mu\text{m}$ sources uncovered (Weiß et al. 2009) had been subtracted using a scaled beam profile.

An important aspect of any stacking analysis performed on maps with coarse angular resolution, is the issue of deblending of sources that lie within a single resolution element. For example, if a BzK galaxy has a neighbour, A, within a LABOCA

beam, we have to calculate the $870\text{-}\mu\text{m}$ flux contribution from A at the position of the BzK galaxy. Of the full $K_{\text{vega}} \leq 20$ sample, we find this to be the case for 5985 sources (i.e. 72 per-cent of the sample). We correct for the blending of sources by assuming Gaussian sources with FWHMs equal to the LABOCA beam. This method is similar to the one adopted by Webb et al. (2004), although they (and subsequent submm stacking studies) did not take into account the effects from neighbour’s neighbours. An illustrative example of the latter is given Fig. 5 where A itself has a neighbour, B, within a LABOCA beam, that is not within the LABOCA beam as measured from the BzK galaxy’s position. In this case we have to calculate B’s contribution to A, in order to correctly calculate A’s contribution to the BzK galaxy, and the system of equations to be solved is therefore

$$f_{\text{BzK}} = I_{\text{BzK}} + I_{\text{A}} e^{-r_{\text{BzK,A}}^2/(2\sigma^2)} \quad (3)$$

$$f_{\text{A}} = I_{\text{A}} + I_{\text{BzK}} e^{-r_{\text{BzK,A}}^2/(2\sigma^2)} + I_{\text{B}} e^{-r_{\text{B,A}}^2/(2\sigma^2)} \quad (4)$$

$$f_{\text{B}} = I_{\text{B}} + I_{\text{A}} e^{-r_{\text{B,A}}^2/(2\sigma^2)} \quad (5)$$

where I and f are the measured and deblended fluxes at the relevant positions, respectively, and r are the distances between the sources. In order to estimate the error one makes by only deblending the fluxes from neighbours within a beam, not taking into account neighbours’ neighbours, we ran the stacking analysis under both scenarios. We find that the deblending scheme by Webb et al. (2004) can overestimate the fluxes by $\sim 10\%$ compared to the scheme described in this paper, but more typically the error is at the $\sim 5\%$ level. We emphasize that one has to not only deblend neighbours within a certain galaxy population, but also across populations. Therefore, the deblending analysis was carried out on the full $K_{\text{vega}} \leq 20$ sample. In doing so we have ignored sources with $K_{\text{vega}} > 20$, and they have therefore not been included in the deblending analysis. In the following section, however, we show that these fainter sources do indeed make a contribution to the submm signal, which must be subtracted from the stacked fluxes.

5.3. Stacking the full samples

For each source in the $K_{\text{vega}} \leq 20$ sample the (deblended) signal and noise values at its pixel position in the LABOCA map were recorded, and

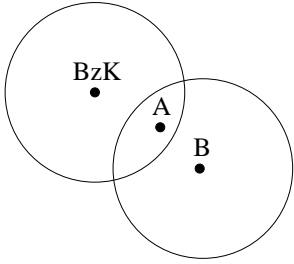


Fig. 5.— An example of where deblending is necessary. In order to properly calculate the 870- μm flux coming from the BzK galaxy at its position we have to calculate A’s contribution, which in turn is affected by B. In total, therefore, a linear set of three equations has to be solved (see eqs. 3-5). The large circles indicate the LABOCA beam.

from those the stacked 870- μm flux density of the full sample was determined according to eqs. 1 - 2. The 870- μm signal and noise values corresponding to the BzK, ERO and DRG samples were extracted and their stacked 870- μm flux densities were derived in a similar manner. In a similar way, postage stamp images around each source were extracted and combined in a weighted fashion resulting in stacked submm-images of the K -selected samples (Fig. 6). From the azimuthally-averaged radial profiles of the submm signal, it is clear that the baseline level is not zero, but in fact there is a residual signal amounting to 0.065 mJy and stemming from the population of $K_{\text{vega}} > 20$ galaxies lying below the submm detection limit of the LABOCA map. In order to account for this effect, the final stacked 870- μm flux densities (Table 2) had a constant signal of 0.065 mJy subtracted from them. As a comparison we also derived the median flux densities from the stacks and found agreement (to within 15 percent) with the weighted averages.

To gauge the significance of our results, we ran a series of Monte Carlo simulations in which stacking analyses were carried out on 1000 versions of the $K_{\text{vega}} \leq 20$ catalogue, each with randomized positions with respect to the original catalogue. Each source was assigned a random position by (randomly) choosing a radius ($60'' \leq r \leq 200''$) and an angle from its original position. By confining the new positions within a certain distance of the original, we ensured that the noise properties were similar to those in the original stacking anal-

ysis. As expected the distributions of stacked signals obtained from these simulations were Gaussians centered on zero. We found that the measured 870- μm signals occurred in $< 0.05\%$ of the simulation runs. Roughly the same percentage is found if we restrict our Monte Carlo analysis to the sBzK, ERO and DRG samples, and clearly testify to the significance of the measured signals.

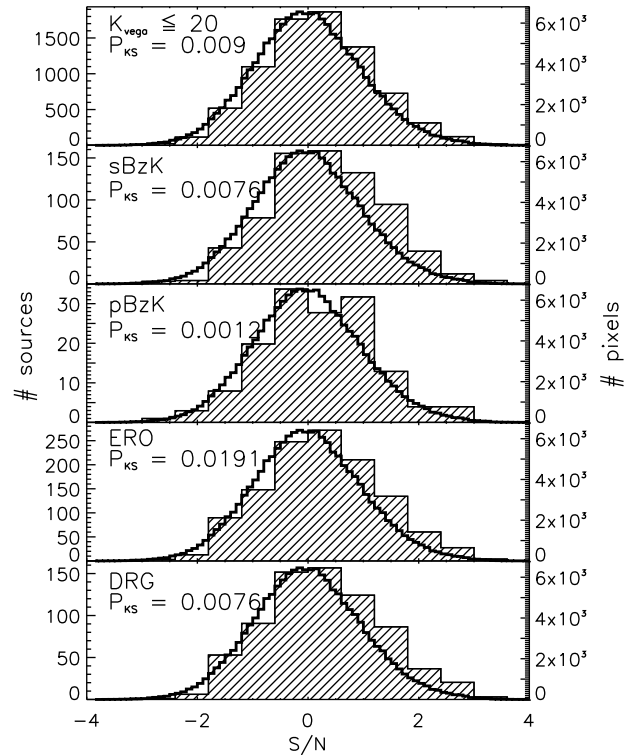


Fig. 7.— The distributions of the S/N values at the positions of the $K_{\text{vega}} \leq 20$ BzK, ERO, and DRG samples, shown as hashed histograms from top to bottom, respectively. The open histograms show the S/N distribution of the residual LABOCA map. The P_{KS} values are the likelihoods that the sample distributions are identical to the overall map distribution.

In addition to the above stacking analysis, we compared the distributions of S/N values at the near-IR source positions with the overall S/N distribution of the residual LABOCA map (Fig. 7). In all cases, a formal Kolmogorov-Smirnov (KS) statistic shows that the sample distributions are statistically different from the distribution of

TABLE 2

THE STACKED 870- μM FLUX DENSITIES FOR THE $K_{\text{vega}} \leq 20$ SAMPLE AS WELL AS THE BzK, ERO, AND DRG SAMPLES. THE NUMBERS OF SOURCES GOING INTO EACH STACK ARE GIVEN IN PARENTHESES ALONG WITH THE SIGNIFICANCE OF THE STACKED SIGNALS. SURFACE DENSITIES AND CONTRIBUTION TO THE 870- μM EBL ARE ALSO LISTED.

Galaxy type	$\langle S_{870\mu\text{m}} \rangle^{\text{a}}$ [mJy]	$\langle S_{870\mu\text{m}} \rangle^{\text{b}}$ [mJy]	$\delta\text{N}^{\text{b}}$ [sq. arcmin $^{-1}$]	$\langle \delta I_{870\mu\text{m}} \rangle^{\text{b}}$ [Jy sq. deg $^{-1}$]
$K_{\text{vega}} \leq 20$	0.19 ± 0.01 (8212, 19.0 σ)	0.20 ± 0.01 (8266, 20.0 σ)	9.18 ± 0.10	6.61 ± 0.34 (15.0 \pm 5.2%)
sBzK	0.38 ± 0.04 (727, 9.5 σ)	0.48 ± 0.04 (744, 12.0 σ)	0.83 ± 0.03	1.70 ± 0.24 (3.9 \pm 1.4%)
pBzK	0.21 ± 0.10 (147, 2.1 σ)	0.27 ± 0.10 (149, 2.7 σ)	0.17 ± 0.01	0.16 ± 0.11 (0.4 \pm 0.3%)
sBzK+pBzK	0.35 ± 0.04 (874, 8.8 σ)	0.45 ± 0.04 (893, 11.3 σ)	0.99 ± 0.03	1.89 ± 0.24 (4.3 \pm 1.6%)
ERO	0.30 ± 0.03 (1225, 10.0 σ)	0.42 ± 0.03 (1253, 14.0 σ)	1.39 ± 0.04	1.85 ± 0.20 (4.2 \pm 1.5%)
DRG	0.32 ± 0.04 (717, 8.0 σ)	0.41 ± 0.04 (737, 10.3 σ)	0.82 ± 0.03	1.09 ± 0.18 (2.5 \pm 0.9%)
BzK/ERO/DRG ^c	0.31 ± 0.03 (1961, 10.3 σ)	0.43 ± 0.03 (1997, 14.3 σ)	2.22 ± 0.05	3.67 ± 0.29 (8.4 \pm 2.9%)
non-BzK/ERO/DRG ^d	0.16 ± 0.01 (6251, 16.0 σ)	0.17 ± 0.01 (6269, 17.0 σ)	6.97 ± 0.09	4.26 ± 0.26 (9.7 \pm 3.3%)
$z < 1.4$				
$K_{\text{vega}} \leq 20$	0.17 ± 0.01 (7026, 17.0 σ)	0.17 ± 0.01 (7055, 17.0 σ)	7.83 ± 0.09	5.36 ± 0.29 (11.7 \pm 4.1%)
sBzK	0.33 ± 0.09 (163, 3.7 σ)	0.42 ± 0.09 (164, 4.7 σ)	0.18 ± 0.01	0.23 ± 0.14 (0.5 \pm 0.4%)
pBzK	-0.03 ± 0.17 (47, -0.18 σ)	-0.14 ± 0.17 (47, -0.8 σ)	0.05 ± 0.01	...
ERO	0.24 ± 0.04 (740, 6.0 σ)	0.26 ± 0.04 (751, 6.5 σ)	0.83 ± 0.03	0.87 ± 0.16 (1.9 \pm 0.7%)
DRG	0.26 ± 0.06 (351, 4.3 σ)	0.29 ± 0.06 (373, 4.8 σ)	0.40 ± 0.02	0.47 ± 0.15 (1.0 \pm 0.4%)
$z > 1.4$				
$K_{\text{vega}} \leq 20$	0.34 ± 0.03 (1186, 11.3 σ)	0.39 ± 0.03 (1211, 13.0 σ)	1.35 ± 0.04	1.89 ± 0.20 (4.1 \pm 1.5%)
sBzK	0.40 ± 0.05 (564, 8.0 σ)	0.55 ± 0.05 (580, 11.0 σ)	0.64 ± 0.03	1.28 ± 0.23 (2.8 \pm 1.1%)
pBzK	0.32 ± 0.12 (100, 2.7 σ)	0.41 ± 0.12 (102, 3.4 σ)	0.11 ± 0.01	0.17 ± 0.16 (0.4 \pm 0.4%)
ERO	0.40 ± 0.05 (485, 8.0 σ)	0.54 ± 0.05 (502, 10.8 σ)	0.56 ± 0.02	1.08 ± 0.22 (2.4 \pm 0.1%)
DRG	0.39 ± 0.06 (366, 6.5 σ)	0.59 ± 0.06 (380, 9.8 σ)	0.42 ± 0.02	0.90 ± 0.23 (1.9 \pm 0.8%)
24- μm detected ($S_{24\mu\text{m}} > 27 \mu\text{Jy}$)				
sBzK	0.55 ± 0.05 (451, 11.0 σ)	0.70 ± 0.05 (466, 14.0 σ)	0.52 ± 0.02	1.30 ± 0.27 (2.8 \pm 1.1%)
pBzK	0.44 ± 0.16 (52, 2.8 σ)	0.54 ± 0.16 (53, 3.4 σ)	0.06 ± 0.01	0.11 ± 0.20 (0.2 \pm 0.4%)
ERO	0.54 ± 0.05 (490, 10.8 σ)	0.68 ± 0.05 (511, 11.6 σ)	0.57 ± 0.03	1.39 ± 0.28 (3.0 \pm 1.0%)
DRG	0.52 ± 0.06 (379, 8.7 σ)	0.73 ± 0.06 (400, 12.2 σ)	0.44 ± 0.02	1.16 ± 0.28 (2.5 \pm 1.0%)
24- μm faint ($S_{24\mu\text{m}} < 27 \mu\text{Jy}$)				
sBzK	0.11 ± 0.07 (276, 1.6 σ)	0.14 ± 0.07 (278, 2.0 σ)	0.31 ± 0.02	0.16 ± 0.09 (0.3 \pm 0.2%)
pBzK	0.08 ± 0.12 (95, 0.7 σ)	0.12 ± 0.12 (96, 1.0 σ)	0.11 ± 0.01	0.05 ± 0.06 (0.1 \pm 0.1%)
ERO	0.14 ± 0.04 (735, 3.5 σ)	0.18 ± 0.04 (742, 4.5 σ)	0.82 ± 0.03	0.53 ± 0.14 (1.2 \pm 0.5%)
DRG	0.10 ± 0.06 (338, 1.7 σ)	0.18 ± 0.06 (344, 3.0 σ)	0.38 ± 0.02	0.25 ± 0.11 (0.5 \pm 0.2%)

NOTE.—^a Submm-faint sources only. ^b Submm-bright sources included. ^c The combined BzK, ERO and DRG samples, where source overlap between the populations have been accounted for.

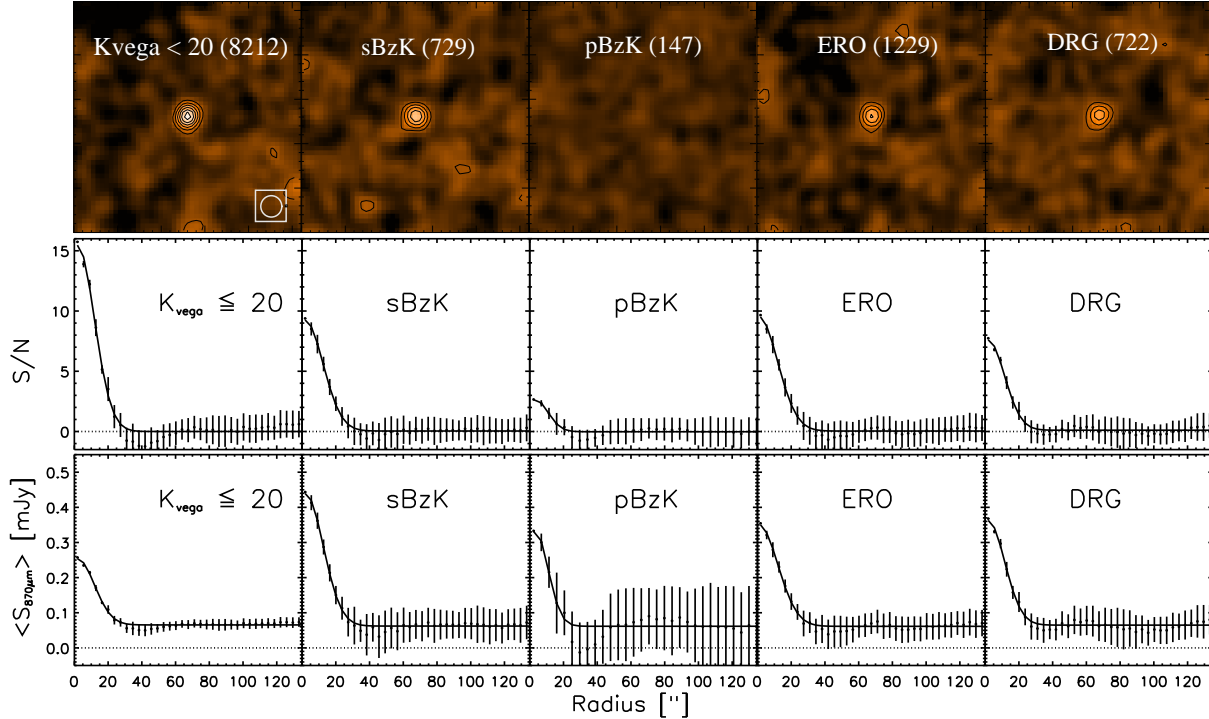


Fig. 6.— **Top row:** Postage stamps of the stacked signal-to-noise images, each $310'' \times 310''$ in size, of the $K_{\text{vega}} \leq 20$, BzK, ERO and DRG samples. The contours start at $S/N = 3$ and increase in steps of 2. The number of sources in each stack is given in parentheses. The angular resolution (FWHM= $27''$) is shown as an insert in the left hand panel. **Middle row:** Radial profiles (azimuthally averaged) of the corresponding stacked S/N images (filled symbols). Gaussian fits to the profiles are indicated by the solid curve. **Bottom row:** Radial profiles (azimuthally averaged) of the corresponding stacked signal images (filled symbols). Gaussian fits to the profiles are indicated by the solid curve. Notice the non-zero baseline level (0.065 mJy) caused by the the $K_{\text{vega}} > 20$ sources with submm fluxes below the detection threshold. This constant baseline level has been removed from the S/N images and profiles in the top and middle panels.

the entire map which is symmetrical around zero (open histogram in Fig. 7). Unlike the distributions for the $K_{\text{vega}} \leq 20$, sBzK, ERO and DRG samples, which are clearly biased towards positive S/N values, the pBzK distribution shows outliers at both positive and negative S/N values. We can therefore not confidently claim a detection even though this is formally suggest by the low KS probability. This is in line with the above analysis which found that the stacked $870\text{-}\mu\text{m}$ signal from pBzKs was not significant.

6. Discussion

6.1. Stacked submm fluxes and star formation rates

In § 5 we found that all of our K -selected samples, except for the pBzKs, have significantly detected stacked $870\text{-}\mu\text{m}$ fluxes. The submm-faint pBzK galaxies are tentatively detected at the $\sim 2\sigma$ -level – as also indicated by the slight increase in the azimuthally averaged S/N radial profile in Fig. 7. How do these compare with previous submm stacking analyses of K -selected samples?

We find average $870\text{-}\mu\text{m}$ flux densities of 0.38 ± 0.04 mJy and 0.21 ± 0.10 mJy for our samples of submm-faint sBzK and pBzK galaxies. In comparison, Daddi et al. (2005) estimated an aver-

age 850- μm signal of $\sim 0.82\text{ mJy}$ (corresponding to a 870- μm signal of $\sim 0.75\text{ mJy}^4$) for a sample of ~ 100 $K_{\text{vega}} \leq 20$ submm-faint sBzK galaxies within the SCUBA map of GOODS-N. Takagi et al. (2007) reported an average 850- μm flux of $0.52 \pm 0.19\text{ mJy}$ (corresponding to a 870- μm flux of $0.48 \pm 0.18\text{ mJy}$) from a sample of 112 $K_{\text{vega}} \leq 20$ sBzK galaxies selected within the part of the Subaru/XMM-Newton deep field (SXDF) covered by the SCUBA HALf Degree Extragalactic Survey (SHADES). Finally, D08 stacked the 850- μm signal from 1421 $K_{\text{vega}} \lesssim 21.7$ sBzK galaxies and found $0.53 \pm 0.06\text{ mJy}$ (corresponding to $0.49 \pm 0.06\text{ mJy}$ at 870- μm). D08 also measured an average 850- μm flux of $0.22 \pm 0.18\text{ mJy}$ (or $0.20 \pm 0.17\text{ mJy}$ at 870- μm) for a sample of 147 $K_{\text{vega}} \lesssim 21.7$ pBzK galaxies.

For the EROs and DRGs we find stacked 870- μm fluxes of $0.30 \pm 0.03\text{ mJy}$ and $0.32 \pm 0.04\text{ mJy}$, respectively. Webb et al. (2004) used the Canada-UK Deep Submillimeter Survey 03hr and 14hr fields (CUDSS03 and CUDSS14, respectively) to perform a 850- μm stacking analysis of 164 $K_{\text{vega}} \lesssim 20.7$ EROs in the two fields, and found a stacked signal for the entire ERO sample of $\langle S_{870\mu\text{m}} \rangle = 0.52 \pm 0.09\text{ mJy}$. Similarly, Takagi et al. (2007) measured a stacked 870- μm signal of $0.49 \pm 0.16\text{ mJy}$ from a sample of 201 $K_{\text{vega}} \leq 20$ EROs selected within SXDF/SHADES. Turning to DRGs, Knudsen et al. (2005) obtained a stacked 850- μm signal of $0.74 \pm 0.24\text{ mJy}$ from a sample of 25 $K_{\text{vega}} \leq 22.5$, submm-faint DRGs (uncorrected for an average gravitational lens amplification of 20%). Converting to a 870- μm flux density and correcting for the lens amplification yields $0.54 \pm 0.18\text{ mJy}$. Takagi et al. (2007) using significantly shallower SCUBA maps failed at detecting a significant 850- μm signal from an average of 67 $K_{\text{vega}} \leq 20$, submm-faint DRGs ($\langle S_{870\mu\text{m}} \rangle = 0.39 \pm 0.23\text{ mJy}$).

We conclude that, within the errors, the previous stacking studies agree well with our results. We also note that our study provide the first robust ($\geq 5\text{-}\sigma$) detection of submm-faint DRGs.

From the stacked submm fluxes we are able to estimate average IR luminosities and star forma-

tion rates (Table 3). IR luminosities are derived by adopting the IR-to-submm SED of Arp 220 and scaling it to the stacked submm fluxes (at the median redshifts derived from the redshift distributions in § 4.2) and integrating it from 8 – 1000 μm . For comparison we also derive IR luminosities assuming that the SEDs are described by modified black-body law with a dust temperature of $T_d = 35\text{ K}$ and $\beta = 1.5$, and integrating from 8 – 1000 μm . Star formation rates (SFR) are derived following Kennicutt (1998): $SFR[M_\odot \text{ yr}^{-1}] = 1.73 \times 10^{-10} L_{\text{IR}}[L_\odot]$. This conversion assumes a Salpeter initial mass function (Salpeter 1955). Of course, we stress that considerable uncertainty is associated with the derived IR luminosities and SFR s since they depend on the assumed SED and IMF.

The average IR luminosities and star formation rates estimated here for $K_{\text{vega}} \leq 20$ sBzK, ERO and DRG galaxies on the basis of their stacked submm fluxes lie in the ranges $\sim 1 - 6 \times 10^{11} L_\odot$ and $\sim 20 - 110 M_\odot \text{ yr}^{-1}$, i.e. comparable to those of LIRGs and ULIRGs in the local Universe. For the sBzK galaxies, the average IR luminosity and star formation rate derived here are fully consistent with UV, 24- μm and radio studies of these galaxies (Daddi et al. 2007). We find that ERO and DRG populations have significantly lower IR luminosities (by $\sim 40\%$) than the sBzK galaxies. This is in part due to the fact that we have made no attempt to weed out passive EROs/DRGs in the stacking analysis, and the stacked submm flux from dusty, starforming EROs/DRGs is likely to be significantly higher.

6.2. Stacking in redshift bins

Using the photometric redshifts obtained in § 4.2 we can stack our samples into separate redshift bins, thereby allowing us to determine which redshifts are contributing the most to the stacked submm signals. Redshift bins were chosen so that they were larger than the typical redshift uncertainty, and provided roughly the same number of sources in each bin. The latter ensured that the same sensitivity was reached in each bin, thus allowing for a direct comparison. Fig. 8 shows the average flux densities of the different samples as a function of redshift. We stress that due to the essentially flat selection function of submm surveys over the redshift range $1 \lesssim z \lesssim 8$ (Blain & Longair

⁴We scale 850- μm fluxes to 870- μm fluxes assuming an optically thin, modified black body law with $\beta = 1.5$, such that: $S_{870\mu\text{m}}/S_{850\mu\text{m}} = (850\mu\text{m}/870\mu\text{m})^{2+\beta} = 0.92$.

TABLE 3

THE AVERAGE IR LUMINOSITIES AND STAR FORMATION RATES OF BzK, ERO AND DRG GALAXIES, DERIVED FROM THEIR STACKED 870- μm FLUXES.

Galaxy type	(z)	L_{IR}^a (Arp 220) [$\times 10^{11} L_{\odot}$]	SFR^b (Arp 220) [$M_{\odot} \text{ yr}^{-1}$]	L_{IR}^a ($T_d = 35 \text{ K}$) [$\times 10^{11} L_{\odot}$]	SFR^b ($T_d = 35 \text{ K}$) [$M_{\odot} \text{ yr}^{-1}$]	L_{IR}^a ($T_d = 30 \text{ K}$) [$\times 10^{11} L_{\odot}$]	SFR^b ($T_d = 30 \text{ K}$) [$M_{\odot} / \text{yr}^{-1}$]
sBzK	1.8	6.3 ± 0.4	109 ± 7	3.7 ± 0.3	65 ± 5	2.1 ± 0.2	37 ± 3
pBzK	1.6	2.9 ± 1.0	50 ± 17	1.7 ± 0.7	30 ± 11	1.0 ± 0.4	17 ± 6
ERO	1.3	3.6 ± 0.3	62 ± 5	2.3 ± 0.2	39 ± 3	1.3 ± 0.1	22 ± 2
DRG	1.4	3.6 ± 0.4	62 ± 7	2.3 ± 0.3	40 ± 4	1.3 ± 0.1	22 ± 3
sBzK ($z < 1.4$)	1.1	3.9 ± 0.8	67 ± 14	2.4 ± 0.5	42 ± 9	1.3 ± 0.3	10 ± 2
sBzK ($z > 1.4$)	2.0	5.8 ± 0.5	101 ± 9	3.9 ± 0.3	67 ± 6	2.3 ± 0.2	39 ± 4
pBzK ($z < 1.4$)	1.2
pBzK ($z > 1.4$)	1.9	4.7 ± 1.2	82 ± 21	3.0 ± 0.8	52 ± 14	1.7 ± 0.5	30 ± 8
ERO ($z < 1.4$)	1.1	2.5 ± 0.4	43 ± 7	1.5 ± 0.2	26 ± 4	0.8 ± 0.1	14 ± 2
ERO ($z > 1.4$)	2.1	5.8 ± 0.5	101 ± 9	3.7 ± 0.3	64 ± 6	2.2 ± 0.2	37 ± 3
DRG ($z < 1.4$)	1.1	2.8 ± 0.6	48 ± 10	1.7 ± 0.3	29 ± 6	0.9 ± 0.2	16 ± 3
DRG ($z > 1.4$)	2.4	5.6 ± 0.6	96 ± 10	3.8 ± 0.4	67 ± 7	2.3 ± 0.2	40 ± 4

^aIR luminosities are obtained by integrating the SED over the wavelength range 8 – 1000 μm .

^bStar formation rates a derived using $SFR[M_{\odot} \text{ yr}^{-1}] = 1.73 \times 10^{-10} L_{\text{IR}}[L_{\odot}]$ (Kennicutt 1998).

1993), the comparison of stacked submm fluxes at different redshifts directly translates into a comparison between far-IR luminosities (and thus star formation rates – Kennicutt 1998) between these redshift bins (to the extent that submm flux is a measure of far-IR luminosity).

The average submm signal from $K_{\text{vega}} \leq 20$ galaxies is found to be roughly constant ($\sim 0.1 - 0.2 \text{ mJy}$) out to $z \sim 1.4$, and consistent with the average flux density of the full sample (Table 2). At $z \sim 1.7$, however, the submm signal has increased to $\sim 0.4 \text{ mJy}$. The stacked submm fluxes of $z < 1.4$ and $z > 1.4$ $K_{\text{vega}} \leq 20$ sources are $0.15 \pm 0.01 \text{ mJy}$ and $0.47 \pm 0.03 \text{ mJy}$, respectively (Table 2). A similar increase in the average submm flux at $z > 1.4$ is seen for the ERO and DRG populations. The average IR luminosities and star formation rate for $z > 1.4$ EROs ($L_{\text{IR}} \simeq 4.9 \times 10^{11} L_{\odot}$ and $SFR \simeq 85 M_{\odot} \text{ yr}^{-1}$) are about $3\times$ higher than for $z < 1.4$ EROs ($L_{\text{IR}} \simeq 1.8 \times 10^{11} L_{\odot}$ and $SFR \simeq 31 M_{\odot} \text{ yr}^{-1}$). For DRGs the difference is about a factor of two: $z > 1.4$ DRGs have on average $L_{\text{IR}} \simeq 4.9 \times 10^{11} L_{\odot}$ and $SFR \simeq 85 M_{\odot} \text{ yr}^{-1}$ while $z < 1.4$ DRGs have $L_{\text{IR}} \simeq 2.4 \times 10^{11} L_{\odot}$ and $SFR \simeq 42 M_{\odot} \text{ yr}^{-1}$. These findings also fit with the ERO and DRG redshift distributions (Fig. 4), where we found evidence for two sub-populations separated at $z \sim 1.6$. Due to our magnitude cut-off at $K_{\text{vega}} \leq 20$, our samples are biased towards increasingly more massive galaxies at higher redshifts. The above results, therefore, suggest that the star formation activity in massive galaxies increase with red-

shift, and that a dominant fraction of massive EROs/DRGs at $z > 1.4$ are actively starforming galaxies, and not old, red galaxies. The less massive EROs and DRGs, which aren't picked up at high- z given the $K_{\text{vega}} \leq 20$ limit, have lower star formation rates, and possibly a higher fraction of evolved, passive galaxies, than the more massive EROs/DRGs. The gradual drop in the average submm signals at $z > 2.5$ is likely a reflection of the incompleteness in our K -band selection at these redshifts.

Turning to the BzK galaxies, we find that sBzKs exhibit a positive and, within the error bars, constant 870- μm signal ($\sim 0.5 \text{ mJy}$) over the redshift range $1 \lesssim z \lesssim 3$. This supports the notion that the sBzK-criterion selects star forming galaxies across this redshift range, and that for our K -band magnitude limit of $K_{\text{vega}} \leq 20$, the distribution of star formation rates of sBzK galaxies is roughly constant within this redshift range. In contrast, the pBzK galaxies show no evidence of significant submm signal in any redshift bin, which is consistent with these galaxies being devoid of significant star formation. D08 reported a 850- μm signal of $0.89 \pm 0.34 \text{ mJy}$ ($\sim 2.6\sigma$) for pBzKs at $z < 1.4$ but no significant signal for pBzKs at $z > 1.4$. They argued that the submm signal for $z < 1.4$ pBzK galaxies was due to contamination by star forming galaxies at $z < 1.4$. In comparison, we find no significant stacked 870- μm signal ($-0.14 \pm 0.17 \text{ mJy}$) for $z < 1.4$ pBzKs and only a marginal signal for $z > 1.4$ pBzKs ($0.36 \pm 0.12 \text{ mJy}$).

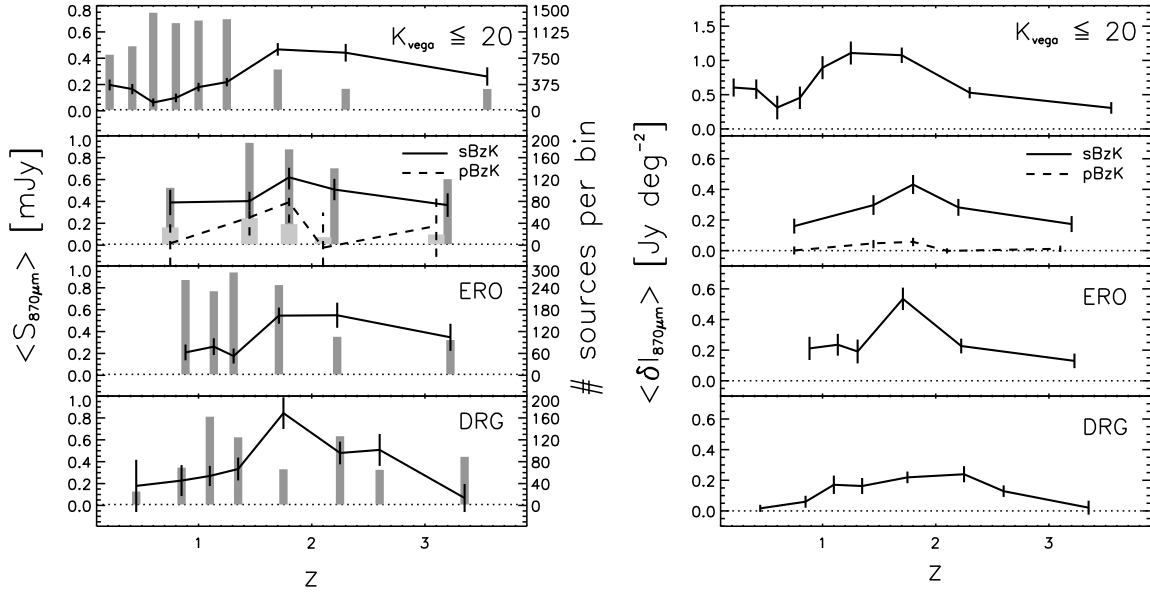


Fig. 8.— Stacked 870- μm flux densities (left panels) and the corresponding contribution to the 870- μm extragalactic background light (right panels) as a function of redshift for the $K_{\text{vega}} \leq 20$, BzK, ERO and DRG samples. The gray histograms in the left hand panels indicate the number of sources in each bin (corresponding y-axis is on the right hand side). Broader, more light-grey histograms have been used for the pBzK galaxies.

6.3. Stacking in 24- μm bins

Using the 24- μm source catalogue from the FIDEL survey (which includes all sources $> 27 \mu\text{Jy}$, $5\text{-}\sigma$ point-source sensitivity – Dickinson et al. in prep), a total of 466/53, 511 and 400 sources in the sBzK/pBzK, ERO and DRG samples, respectively, were identified at 24- μm . Their average submm fluxes are given in Table 2 along with those of the 24- μm faint ($< 27 \mu\text{Jy}$) subsets. The 24- μm detected subsets have $\gtrsim 5\times$ higher average submm flux densities than the 24- μm faint sources. This is not surprising since the mid-IR is known to trace the thermal dust emission, and one might even expect a correlation between the submm and mid-IR emission.

In order to investigate the latter, we measured the stacked 870- μm signal as a function of 24- μm flux density bins (Fig. 9). The sBzK, ERO and DRG galaxies all exhibit a similar behaviour, namely a significant linear correlation between the stacked 870- μm and 24- μm flux density up to $S_{24\mu\text{m}} \simeq 350 \mu\text{Jy}$, given by $\langle S_{870\mu\text{m}} \rangle =$

$4.5 \times 10^{-3} \langle S_{24\mu\text{m}} \rangle$, followed by a flattening of the relation for $S_{24\mu\text{m}} > 350 \mu\text{Jy}$. Not surprisingly, the pBzKs are not significantly detected at 870- μm in any of the 24- μm bins, and no submm-mid-IR correlation is seen.

Although the 24- μm selection function (Daddi et al. 2007) depends strongly on redshift (unlike the selection function at submm wavelengths), the observed $S_{24\mu\text{m}} - S_{870\mu\text{m}}$ correlation strongly suggests that 24- μm measurements (with $S_{24\mu\text{m}} \gtrsim 350 \mu\text{Jy}$) trace systems dominated by star formation, and can be used to derive IR luminosities and star formation rates. The constant $S_{870\mu\text{m}} \simeq 1.3 \text{ mJy}$ ratio for $S_{24\mu\text{m}} \simeq 350 - 1000 \mu\text{Jy}$ is likely to reflect significant contamination by an AGN at these high 24- μm flux densities. Since the mid-IR will be more sensitive to warm dust ($T_d \sim 80 - 200 \text{ K}$) than the submm, which largely traces cold dust ($T_d \sim 20 - 60 \text{ K}$), the ability of the observed 24- μm emission to reliably trace IR luminosity and star formation may be compromised by AGN-heated warm dust. The turn-over from a linear to a flat $S_{870\mu\text{m}} - S_{24\mu\text{m}}$ relation occurs

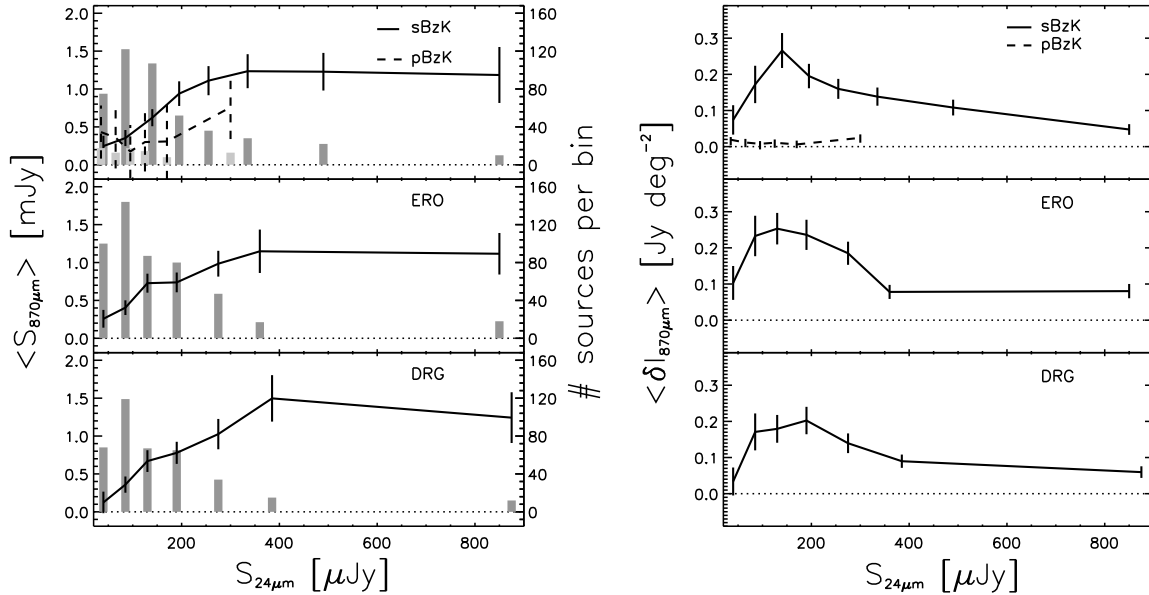


Fig. 9.— Stacked 870- μm flux densities (left panels) and the corresponding contribution to the 870- μm extragalactic background light (right panels) as a function of 24- μm flux density for the BzK, ERO and DRG samples. The gray histograms in the left hand panels indicate the number of sources in each bin (corresponding y-axis is on the right hand side). Broader, more light-grey histograms have been used for the pBzK galaxies. In all cases, a significant $S_{870\mu\text{m}} - S_{24\mu\text{m}}$ correlation is found for $S_{24\mu\text{m}} \lesssim 350 \mu\text{Jy}$, indicating that across this flux range, 24- μm observations trace star formation. For $S_{24\mu\text{m}} \gtrsim 350 \mu\text{Jy}$, however, the relation flattens, suggestive of an increase in the fraction of AGN-dominated systems.

at $S_{24\mu\text{m}} \simeq 350 \mu\text{Jy}$, which corresponds to $L_{\text{IR}} < 1.5 \times 10^{12} L_{\odot}$ at $z \sim 2$.

Our findings are in line with those of Papovich et al. (2007), who found that IR luminosities derived from 24-, 70-, and 160- μm *Spitzer* data (of a sample of K -selected galaxies at $1.5 \lesssim z \lesssim 2.5$ with $S_{24\mu\text{mJy}} \simeq 50 - 250 \mu\text{Jy}$) were in good agreement with those derived from 24- μm data alone. For sources with $S_{24\mu\text{mJy}} > 250 \mu\text{Jy}$, however, the latter would be $\sim 2 - 10\times$ higher, suggesting that the AGN may contribute significantly to the high 24- μm emission. Similarly, Daddi et al. (2004, 2005) found that a large fraction ($> 30\%$) of sBzK galaxies with $L_{\text{IR}} \gtrsim 1.5 \times 10^{12} L_{\odot}$ (which corresponds to the IR luminosity where we find a turn-over in the $S_{870\mu\text{m}} - S_{24\mu\text{m}}$ relation) show an excess of emission in the near-IR (rest-frame) and are statistically detected in hard X-rays – evidence of powerful AGN in these very IR-luminous systems.

6.4. Contributions to the extragalactic background light

Turning to the contribution to the submm extragalactic background light (EBL) by the different populations, we adopt the spectral approximations to the EBL at submm wavelengths from COBE/FIRAS (Puget et al. 1996; Fixsen et al. 1998), including their uncertainties. In doing so we adopt a value of the EBL at 870- μm of $44 \pm 15 \text{ Jy deg}^{-2}$. From the surface densities of the samples we derive their contributions to the 870- μm extragalactic background light (Table 2). We find that the total contribution from all $K_{\text{vega}} \leq 20$ sources to the 870- μm EBL is $6.61 \pm 0.34 \text{ Jy deg}^{-2}$, or $15.0 \pm 5.2\%$. For the BzK galaxies we find that the passive ones contribute $\lesssim 1\%$ to the 870- μm EBL, while the star forming population contribute $1.70 \pm 0.24 \text{ Jy deg}^{-2}$, corresponding to $3.9 \pm 1.4\%$. The EROs contribute a similar amount to the EBL at 870- μm as the sBzK galaxies ($1.85 \pm 0.20 \text{ Jy deg}^{-2}$ or $4.2 \pm 1.5\%$), while the contribu-

tion from DRGs, owing to their lower surface density, is about 80% smaller ($1.09 \pm 0.18 \text{ Jy deg}^{-2}$ or $2.5 \pm 0.9 \%$). The combined BzK/ERO/DRG sample, which includes the bulk of massive starforming galaxies at $z \gtrsim 1$, contribute with $8.4 \pm 2.9 \%$ to the EBL at $870\text{-}\mu\text{m}$ after accounting for overlap between the populations.

According to Takagi et al. (2007) sBzK galaxies down to $K_{\text{vega}} \lesssim 20$ contribute with $3.8 \pm 1.2 \text{ Jy deg}^{-2}$ (or $8.3 \pm 3.9 \%$) to the background light at $850\text{-}\mu\text{m}$ ($46 \pm 16 \text{ Jy deg}^{-2}$ – Puget et al. 1996; Fixsen et al. 1998). Webb et al. (2004) found that the ERO population down to $K_{\text{vega}} < 20.7$ constitutes 7-11% of the EBL at $850\text{-}\mu\text{m}$, while Takagi et al. (2007) reported a $850\text{-}\mu\text{m}$ EBL contribution from $K_{\text{vega}} \lesssim 20$ EROs of $5.1 \pm 1.5 \text{ Jy deg}^{-2}$ ($11 \pm 5 \%$) to the total background at $850\text{-}\mu\text{m}$. Knudsen et al. (2005) found that DRG galaxies down to $K_{\text{vega}} < 22.5$ contribute $\sim 7.7 \text{ Jy deg}^{-2}$ ($\sim 17 \%$) of the EBL at $850\text{-}\mu\text{m}$.

Next, let us look at the contribution to the EBL at $870\text{-}\mu\text{m}$ from the different samples as a function of redshift and $24\text{-}\mu\text{m}$ flux bins (right panels in Fig. 8 & 9). We calculate the contributions using the stacked submm flux and the surface density of sources in each redshift and $24\text{-}\mu\text{m}$ bin.

Looking at the redshift dependence first, we see that the strongest contribution to the $870\text{-}\mu\text{m}$ EBL by $K_{\text{vega}} \leq 20$ galaxies in a given redshift bin, is coming from sources in the redshift range $1 < z < 2$ – they contribute with $7.3 \pm 0.2 \text{ Jy deg}^{-2}$ to the submm EBL, which corresponds to $\sim 50 \%$ of the total contribution from $K_{\text{vega}} \leq 20$ galaxies (Table 2). Although $K_{\text{vega}} \leq 20$ galaxies at $z > 2$ have significant submm emission (§ 6.2), their low abundance means that they contribute $\lesssim 1 \%$ to the observed submm EBL. In contrast, $z < 1$ $K_{\text{vega}} \leq 20$ galaxies are abundant (Fig. 4), but their low average submm fluxes implies a $\lesssim 1 \%$ contribution to the submm EBL.

The bulk ($\sim 80 \%$) of the contribution to the submm EBL from $24\text{-}\mu\text{m}$ detected (i.e. $S_{24\mu\text{Jy}} > 27 \mu\text{Jy}$) sBzK, ERO and DRG galaxies comes from sources with $S_{24\mu\text{Jy}} \simeq 50 - 350 \mu\text{Jy}$, with only a minor fraction coming from brighter, presumably, AGN-dominated sources.

6.5. Stacking across the BzK and RJK diagrams

The sBzK and pBzK selections are designed to locate star forming and passive galaxies in the redshift range $1.4 \leq z \leq 2.5$, while the ERO and DRG colour criteria are designed to select extremely red (either due to dust extinction or old age) galaxies at $z > 1$. Still, the exact definitions of these colour criteria are somewhat arbitrary. Given the large number of sources available to us, we are in a position to construct stacks of the $870\text{-}\mu\text{m}$ signal from statistically significant subsets of galaxies across the BzK and RJK diagrams, thus allowing us to see where in these colour-colour diagrams the submm signal is coming from. Ultimately, this may allow us to fine-tune the sBzK/pBzK criteria, as well as potentially identify regions of the RJK-diagram containing dusty/starforming vs. old/passive EROs and DRGs.

In Fig. 10 and 11 we show the signal- and S/N -contours of the stacked $870\text{-}\mu\text{m}$ signal obtained across the BzK- and RJK-diagrams, where the stacking has been carried out within equally sized grid-cells. We have done this for the full sample, as well as for subsets of the sample within the redshift intervals $0 < z < 0.8$, $0.8 < z < 1.5$, and $1.5 < z < 3.0$. These intervals were motivated by the redshift distributions in Fig. 4, which showed evidence of distinct populations between $0.8 < z < 1.5$ and $1.5 < z < 3.0$.

Considering Fig. 10a first, we see that the sBzK criterion by Daddi et al. (2004) seems to be robust in the sense that the bulk of the $870\text{-}\mu\text{m}$ signal is emerging from the sBzK region. Comparing with Fig. 1a indicates that virtually the entire submm signal is coming from the subset of sBzK galaxies (with a slight overlap into the pBzK and non-BzK regions), which have also been classified as EROs. Due to their extremely red colours and relatively strong submm signal, these galaxies are very likely to be amongst the most dusty, star forming sources of the submm-faint $K_{\text{vega}} \leq 20$ selected galaxies, yet their brightness ensures that they are detected in the blue (thus qualifying as sBzK galaxies).

The submm signal clearly extends into the pBzK region suggesting that some contamination by star forming galaxies occurs. This is partly due the low density of sources in the pBzK-region

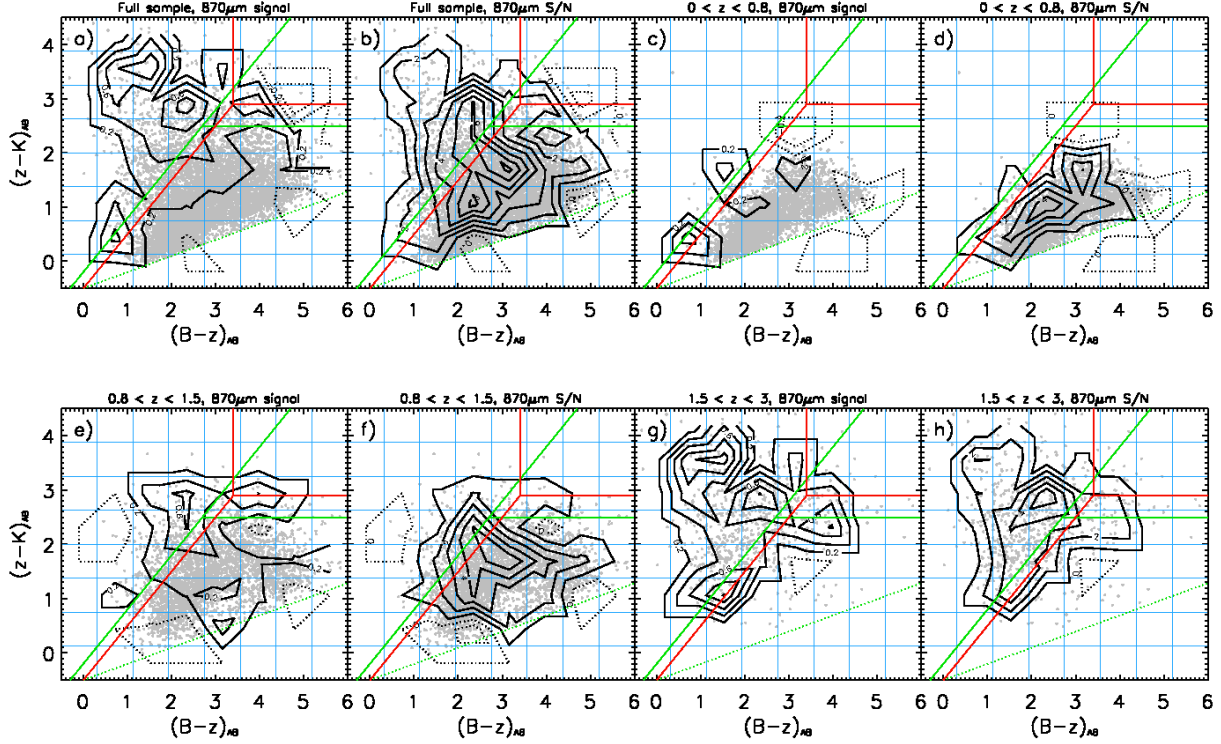


Fig. 10.— Contours of the stacked $870\text{-}\mu\text{m}$ signal (in units of mJy) and S/N across the BzK diagram, obtained by stacking the submm flux in a regular grid (shown in blue). We have stacked the entire sample within the full redshift range, as well as subsets within the redshift ranges $z = 0 - 0.8$, $0.8 - 1.5$, and $1.5 - 3.0$. The sBzK- and pBzK-criteria by Daddi et al. (2004) are shown as solid green lines, while the refined selection criteria proposed in this paper are shown in red. The contours clearly supports the BzK-selection technique as the submm signal is seen to be almost entirely dominated by sBzK galaxies in the redshift range $z = 1.5 - 3$.

which implies that more sources will scatter into the region (due to photometric errors) than out of it. Based on the $870\text{-}\mu\text{m}$ signal and S/N contours in Fig. 10, we propose a refinement of the sBzK and pBzK criteria, namely

$$(z - K)_{AB} \geq (B - z)_{AB} - 0.5 \quad (6)$$

$$(B - z)_{AB} \leq 3.4 \quad (7)$$

for sBzKs, and

$$(z - K)_{AB} \geq 2.9 \quad (8)$$

$$(B - z)_{AB} > 3.4 \quad (9)$$

for pBzKs.

That these refined selection criteria might do a better job at selecting starforming and passive

BzK galaxies, is confirmed if we consider how the submm signal across the BzK-diagram changes with redshift (Fig. 10c-h). We find that only marginal $870\text{-}\mu\text{m}$ emission emerges from galaxies in the redshift interval $0 < z < 0.8$, while in the $0.8 < z < 1.5$ interval, significant submm emission (~ 0.6 mJy) starts to appear from galaxies lying within the sBzK region. At $1.5 < z < 3$ a strong submm signal (~ 1 mJy) and nearly all of the submm emission is coming from the sBzK region. This observed migration of the stacked submm signal towards the sBzK region as a function of redshift, illustrates the ability of the sBzK-criterion to select starforming galaxies at $z \geq 1.5$.

Turning to the RJK-diagram, the bulk of the submm-signal is found to come from the overlap

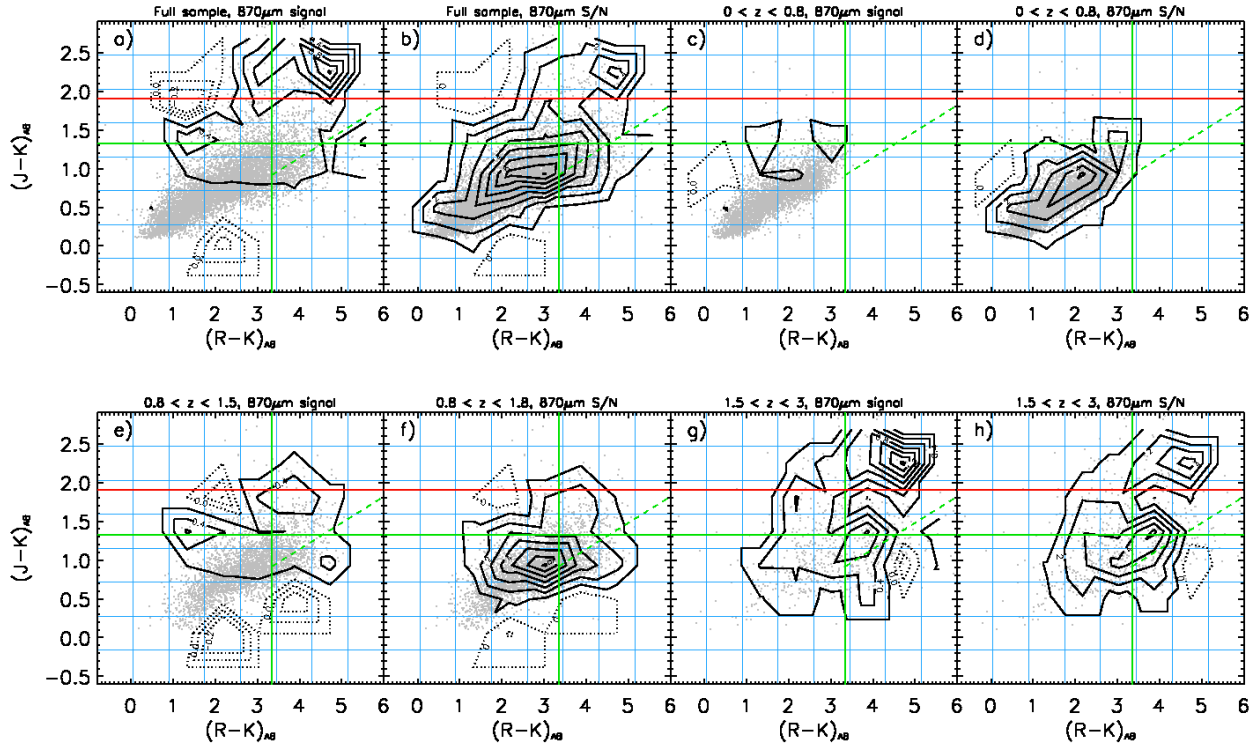


Fig. 11.— Contours of the stacked $870\text{-}\mu\text{m}$ signal (in units of mJy) and S/N across the RJK diagram, obtained by stacking the submm flux in a regular grid (shown in blue). We have stacked the entire sample within the full redshift range, as well as subsets within the redshift ranges $z = 0 - 0.8$, $0.8 - 1.5$, and $1.5 - 3.0$. The ERO- and DRG-criteria are shown as vertical and horizontal solid green lines, while the starforming vs. passive ERO criterion proposed by Pozzetti & Mannucci (2000) is illustrated by the green dashed line (with starforming and passive EROs lying above and below the line, respectively). The strongest submm signal is coming from galaxies in the redshift range $z = 1.5 - 3$ lying in the DRG-ERO overlap region.

region between DRGs and EROs, in particular from ERO/DRG galaxies with $(J - K)_{AB} > 1.9$. The latter, together with the tentative evidence of an underdensity of sources at $(J - K)_{AB} = 1.9$ (see Fig. 1), suggests that $(J - K)_{AB} > 1.9$ may be a useful criterion for selecting a dusty, starforming galaxies. This is strengthened by the fact that the submm signal becomes even stronger and further concentrated towards the ERO/DRG overlap region if we consider only the subset of sources at $z = 1.5 - 3$ (Fig. 11g-h). In the redshift range $0.8 < z < 1.5$, the submm signal is much weaker (~ 0.6 mJy) and comes from ERO/DRG galaxies with $(J - K)_{AB} < 1.9$.

It is well-known that the $K_{\text{vega}} \leq 20$ ERO population is a heterogeneous population, consisting

of roughly a fifty-fifty mix of dusty, star forming EROs and evolved, passive EROs (Spinrad et al. 1999; Dey et al. 1999; Cimatti et al. 1999; Mannucci et al. 2002). Pozzetti & Mannucci (2000) argued that a crude separation between the two types of EROs could be made based on the criterion $(J - K)_{AB} = 0.34(R - K)_{AB} - 0.22$ (and $(R - K_S)_{AB} \geq 3.35$)⁵, with dusty, star forming EROs lying above the relation and old, passive EROs below it. While our stacking analysis lends some merit to the Pozzetti & Mannucci criterion, as the bulk of the submm signal is clearly found above it, significant submm emission is also detected in the passive ERO region (in particular for

⁵We have converted the Pozzetti & Mannucci criterion, which was in the vega system, into AB magnitudes.

sources at $z > 1.5$), suggesting that blindly applying the criterion does not produce clean samples of starforming and passive EROs (see also Smail et al. 2002b).

Finally, we caution that by adopting equally sized grid cells, some cells will contain a significantly larger number of sources than others, thereby introducing a potential skewing of the measured S/N across the diagrams (which is why we also show the variation of the average submm flux density across the diagrams). As a check on our results, we therefore adopted two alternative methods for binning the sources. First, an adaptive mesh was applied by requiring that no more than 200 sources were allowed within a given cell, and, secondly, the 50 nearest neighbours of each source were identified and stacked. Reassuringly, the two additional binning methods gave results in good agreement with the regular grid results.

7. Summary

Using the APEX/LABOCA 870- μm map of the ECDF-S (Weiß et al. 2009) along with the publically available MUSYC survey data of this field (Taylor et al. 2008), we have performed a submm stacking analysis of 8266 K -band selected ($K_{\text{vega}} \leq 20$) galaxies, as well as subsets of 737 DRG, 1253 ERO, and 744/149 sBzK/pBzK galaxies. Photometric redshifts have been derived for the full $K_{\text{vega}} \leq 20$ sample using $UBVRIzJHK$ data from MUSYC, thereby allowing us to study stacked submm flux densities as a function of redshift. This represents the largest submm stacking analyses of near-IR selected galaxies to date. The main results are summarized below:

- We measure stacked 870- μm signals of $0.20 \pm 0.01 \text{ mJy}$ (20.0σ), $0.45 \pm 0.04 \text{ mJy}$ (11.3σ), $0.42 \pm 0.03 \text{ mJy}$ (14.0σ), and $0.41 \pm 0.04 \text{ mJy}$ (10.3σ) for the $K_{\text{vega}} \leq 20$, BzK, ERO and DRG samples, respectively. Splitting the BzK galaxies up into star-forming (sBzK) and passive (pBzK) galaxies, the former is significantly detected ($0.48 \pm 0.04 \text{ mJy}$, 12.0σ) while the latter, as expected, is not ($0.27 \pm 0.10 \text{ mJy}$, 2.7σ). This implies that $K_{\text{vega}} \leq 20$ galaxies are responsible for $15 \pm 5\%$ of the EBL at 870- μm . sBzK galaxies, EROs and DRGs (brighter than $K_{\text{vega}} \leq 20$) are found to contribute $\sim 4\%$ of the 870- μm back-

ground each.

- Performing the stacking analysis in redshift bins, it is found that the stacked submm signal from $K_{\text{vega}} \leq 20$ galaxies, as well as the ERO and DRG sub-samples, is coming from sources in the redshift range $1.4 \lesssim z \lesssim 2.5$, while for BzK galaxies the signal remains constant with redshift. Assessing the contribution to the submm EBL from the different samples as a function of redshift is complicated by the fact that these are flux-limited samples, although, we can conclude that the bulk of the submm light from $K_{\text{vega}} \leq 20$ galaxies comes from sources at $z > 1$.

- We find a linear correlation between stacked submm flux and 24- μm flux density for sBzK, ERO and DRG galaxies with $S_{24\mu\text{m}} \lesssim 350 \mu\text{Jy}$. This correlation suggests that the 24- μm emission from $S_{24\mu\text{m}} \lesssim 350 \mu\text{Jy}$ galaxies is dominated by star formation, and consequently can be used as a robust tracer of star formation. At $S_{24\mu\text{m}} > 350 \mu\text{Jy}$ we find that the stacked 870- μm flux density becomes constant ($\sim 1.3 \text{ mJy}$) and independent of $S_{24\mu\text{m}}$, which is likely due to AGN starting to contribute significantly to the 24- μm as well as 870- μm emission.

- In an effort to isolate a subset of BzK, ERO, and DRG galaxies responsible for the bulk of the stacked 870- μm emission we have measured the significance of the stacked submm signal across the BzK and RJK diagrams, identifying the regions of strongest submm emission. We find that the stacked submm signal from submm-faint sBzK galaxies is dominated by the subset of sources which also fulfill the ERO criterion. These are likely to be dusty, starforming galaxies, which are sufficiently bright in the blue to be selected as sBzK galaxies. The majority of these sources are found in the redshift range $z = 1.5 - 3$, in line with the BzK-selection criterion proposed by Daddi et al. (2004). Guided by the stacked submm-contours we propose slightly modified BzK-selection criteria, namely

$$(z - K)_{\text{AB}} \geq (B - z)_{\text{AB}} - 0.5 \quad (10)$$

$$(B - z)_{\text{AB}} \leq 3.4 \quad (11)$$

$$(12)$$

for sBzKs, and

$$(z - K)_{AB} \geq 2.9 \quad (13)$$

$$(B - z)_{AB} > 3.4 \quad (14)$$

$$(15)$$

for pBzKs.

In the RJK-diagram we find that the strongest submm signal comes from galaxies in the ERO/DRG overlap region with $(J - K)_{AB} > 1.9$, which are predominantly found at $z \geq 1.5$.

We are grateful to Loretta Dunne and Ryan Quadri for providing us with the photometric redshift distributions published in D08 and Q07. IRS acknowledges support from the Royal Society and STFC. TRG is grateful to the European Southern Observatory (ESO) for sponsoring a 4 months visit in Garching during which much of the analysis presented here was carried out, and would in particular like to thank Sune Toft, Carlos de Breuck and Jesper Sommer-Larsen for useful discussions and suggestions during this period.

REFERENCES

- Alexander D.M., et al. 2003, AJ, 126, 539
- Barger A.J., Cowie L.L., Sanders D.B., Fulton E., Taniguchi Y., Sato Y., Kawara K., Okuda H. 1998, Nature, 394, 248
- Barger A.J., Cowie L.L., Sanders D.B. 1999, ApJ, 518, L5
- Bertoldi F., et al. 2007, ApJS, 172, 132
- Blain A.W. & Longair M.S. 1993, MNRAS, 264, 509
- Blain A.W., et al. 1999, ApJ, 512, L87
- Blain A.W., Smail Ian, Ivison R.J., Kneib J.-P., Frayer, D.T. 2002, PhR, 369, 111
- Bolzonella M., Miralles J.-M., Pellò R. 2000, A&A, 363, 476
- Brammer G.B., van Dokkum P.G., Coppi P. 2008, ApJ, 686, 1503
- Chapman S.C., Blain A.W., Ivison R.J., Smail Ian 2003, Nature, 422, 695
- Chapman S.C., Blain A.W., Smail Ian, Ivison R.J. 2005, ApJ, 622, 772
- Cimatti A., et al. 1999, A&A, 352, L45
- Cimatti A., et al. 2002, A&A, 391, L1
- Cimatti A., et al. 2003, A&A, 412, L1
- Cimatti A., et al. 2008, A&A, 482, 21
- Coppin K., et al. 2006, MNRAS, 372, 1621
- Daddi E., et al. 2004, ApJ, 617, 746
- Daddi E., et al. 2005, ApJ, 631, L13
- Daddi E., et al. 2007, ApJ, 670, 156
- Damen M., et al. 2009, ApJ, 690, 937
- Dunne L., et al. 2008, MNRAS, in press
- Elston R., Rieke G.H., Rieke M.J. 1988, ApJ, 331, L77
- Fixsen D.J., Dwek E., Mather J.C., Bennett C.L., Shafer R.A. 1998, ApJ, 508, 123
- Franx M., et al. 2003, ApJ, 587, L79

- Gawiser E., et al. 2003, AAS, 205, 8104
- Gawiser E., et al. 2006, ApJS, 162, 1
- Giavilsco M., et al. 2004, ApJ, 600, L93
- Hu E.M. & Ridgway S.E. 1994, AJ, 107, 1303
- Hughes D.H., et al. 1998, Nature, 394, 241
- Kong X., et al. 2006, ApJ, 638, 72
- Knudsen K.K., et al. 2005, ApJ, 632, L9
- Knudsen K.K., van der Werf P.P., Kneib J.-P. 2008, MNRAS, 384, 1611
- Kriek M., et al. 2006, ApJ, 649, L71
- Kriek M., et al. 2008, ApJ, 677, 219
- Lawrence A., et al. 2007, MNRAS, 379, 1599
- Lehmer B.D., et al. 2005, ApJS, 161, 21
- Luo B., et al. 2008, ApJS, 179, L19
- McCarthy P.J., Persson S.E., West S.C. 1992, ApJ, 386, 52
- Popesso P., et al. 2008, A&A, submitted
- Puget J.-L., Abergel A., Bernard J.-P., Boulanger F., Burton W.B., Desert F.-X., Hartmann D. 1996, A&A, 308, L5
- Rix H.-W., et al. 2004, ApJS, 152, 163
- Quadri R., et al. 2007, AJ, 134, 1103
- Siringo, G., et al. 2009, A&A, in press
- Smail Ian, Ivison R.J., Blain A.W. 1997, ApJ, 490, L5
- Smail Ian, Ivison R.J., Blain A.W., Kneib J.-P. 2002a, MNRAS, 331, 495
- Smail Ian, Owen F.N., Morrison G.E., Keel W.C., Ivison R.J., Ledlow M.J. 2002b, ApJ, 581, 844
- Spergel D.N., et al. 2003, ApJS, 148, 175
- Szokoly G.P., et al. 2004, ApJS, 155, 271
- Takagi T., et al. 2007, MNRAS, 381, 1154
- Taylor E., et al. 2008, ApJ, in press
- van Dokkum P.G., et al. 2003, ApJ, 587, L83
- Vanzella E., et al. 2005, A&A, 434, 53
- Vanzella E., et al. 2006, A&A, 454, 423
- Vanzella E., et al. 2008, A&A, 478, 83
- Webb T.M.A., Brodwin M., Eales S., Lilly S.J. 2004, ApJ, 605, 645
- Wolf C., Dye S., Kleinheinrich M., Meisenheimer K., Rix H.-W., Wisotzki L. 2001, A&A, 377, 442
- Yan L., Thompson D., Soifer B.T. 2004, AJ, 127, 1274

This 2-column preprint was prepared with the AAS L^AT_EX macros v5.2.